Ex vivo modelling of lung tissue resident antimicrobial responses

Hélèna Choltus[1], Julien Prados[2#], Niccolo Bianchi[3#], Nelli Heikkila[4], Wolfram Karenovics[5], Veronique Serre Beinier[6], Nina Leitner[1], Benoit Bédat[5], Fedor Bezrukov[1], Beryl Mazel-Sanchez[7], Virginie Prendki[8], Alexander Lobrinus[9,10], Christiane Eberhardt[3,4,11], Simone Becattini[3,12], Mirco Schmolke[1,12*]

[1] Dept of Microbiology and Molecular Medicine, Medical Faculty, University of Geneva, Switzerland
[2] Bioinformatics Core Facility, Medical Faculty, University of Geneva, Switzerland
[3] Dept of Pathology and Immunology, Medical Faculty, University of Geneva, Switzerland
[4] Dept of Pediatrics, Gynecology and Obstetrics, University Hospital of Geneva (HUG), Switzerland
[5] Thoracic and Endocrine Surgery Division, University Hospitals Geneva (HUG), Switzerland
[6] Dept of Surgery, Medical Faculty, University of Geneva, Switzerland
[7] National reference center for influenza (CNRI), University Hospitals Geneva (HUG), Switzerland
[8] Department of Rehabilitation and Geriatrics, Geneva University Hospitals, Geneva, Switzerland.
[9] Institute of Pathology, Lausanne University Hospital (CHUV), Lausanne, Switzerland.
[10] Department of Clinical Pathology, University Hospital Geneva, Geneva, Switzerland.
[11] Center for Vaccinology, Medical Faculty, University of Geneva, Switzerland
[12] Geneva Center for Inflammation research, Medical Faculty, University of Geneva, Switzerland

* corresponding author
# equal contribution
(contact: mirco.schmolke@unige.ch)

Keyworks: PCLS, precision cut lung slices, *ex vivo* model, preclinical model, antimicrobial, innate immunity, influenza virus, *Streptococcus pneumoniae*, 3R, infectious disease, interferon, interleukin

Abstract:

Tissue resident host responses to microbial infections in the respiratory tract are highly dynamic in space and time and rely on the interaction of a multitude of cell types. In an attempt to model these multicellular responses reliably in cell culture, we compare here the global transcriptional antimicrobial response to infection with influenza A virus (IAV) in precision cult lung slices (PCLS), volume defined organ discs largely maintaining the cellular composition and 3D architecture of the donor lung. To permit a fair comparison of host responses in an isogenic background we first challenged mice in vivo and murine PCLS (mPCLS) and assess host transciptomic changes by unbiased RNAseq. While core antiviral responses overlapped substantially, mPCLS lacked certain features—such as type II interferon expression—likely due to the absence of infiltrating immune cells responses. Importantly, when expanding our findings to immune experienced human precision cut lung slices (hPCLS), we find a much broader antiviral response after IAV challenge, including type I, II and III interferons, suggesting the presence of responsive tissue resident lymphocytes. To prove specificity of this response we infected hPCLS with Streptococcus pneumoniae. Ex vivo tissues responded with a distinct proinflammatory gene profile including IL1A, IL1B and IL17 expression. Blocking of IL-1 signaling partially inhibited the proinflammatory response, suggesting cellular cross-talk and a complex and specific antimicrobial reaction in this *ex vivo* model. In conclusion diversified tissue resident immune cell compartment distinguishes the human *ex vivo* model, making it an ideal system for microbiological and immunological research.

53 **Importance**

54 Pathogen interactions with the lung are very dynamic processes. In biomedical research it is
55 paramount to model these processes in the laboratory as accurately as possible. Influenza A
56 virus has been extensively studied in epithelial cell culture models, including advanced
57 organoids and organ on a chip systems. We use here ex vivo cultured PCLS and use
58 transcriptomics to assess the global tissue resident host response to viral and bacterial
59 challenge. Our data show 1) that murine PCLS faithfully reflect core responses to viral
60 infection, while missing proinflammatory responses linked to infiltrating immune cells and 2)
61 that human PCLS show a highly diversified tissue resident immune response to viral infection
62 due to previous exposures of the host to this pathogen. These responses are clearly distinct
63 from antibacterial gene profiles. Our data advertise PCLS as a complex and realistic model to
64 study tissue resident immune responses to microbes in a human system.

65

66 **Introduction**

67 Respiratory infections with viral or bacterial pathogens are the 5th leading cause of death
68 worldwide and the leading cause of death in low income countries (excluding COVID-19)
69 according to 2021 WHO estimations[1]. Continuous exposure to the surrounding air makes the
70 lung mucosa an ideal entry port for airborne viral and bacterial pathogens. Influenza viruses
71 alone are responsible for more than half a million deaths annually often complicated by
72 secondary bacterial pneumonia, mostly with Streptococcus pneumoniae or Staphylococcus
73 aureus. A major initial barrier against establishment of respiratory infections is the
74 antimicrobial host response elicited by respiratory epithelial cells in conjunction with tissue
75 resident immune cells. Modelling the complexity of this first line of defense in cell culture
76 setting remains however challenging, in part since the human lung consists of more than fifty

77 cell types[2]. 2D cell culture models do not reflect this cellular diversity and the complex spatial
78 3D organization of respiratory tissue.
79 Precision cut lung slices (PCLS) are *ex vivo* cultured, i.e. volume defined discs of human or
80 animal lung tissue origin and bridge conventional cell culture models and *in vivo* systems [3,4].
81 They preserve the cellular composition and 3D architecture of lung tissue and are arguably
82 the most complex *ex vivo* model to study lung physiology and pathology[5]. Since they are
83 disconnected from the circulation of the host organism, they constitute an ideal scenario to
84 study the tissue resident immune response to invading microbes. We compare here the tissue
85 resident host response to viral and bacterial challenge in a murine and human ex vivo model
86 with data from in vivo infected lung tissues.
87
88 **Results**
89 The antiviral host response to influenza A viruses in the respiratory tract is an
90 extraordinarily dynamic process initiated by infected epithelial cells and surveilling tissue
91 resident immune cells. This first line of defense can be decisive for the outcome of infection.
92 It establishes an antiviral state in the respiratory tissue, most importantly induced by
93 cytokines of the interferon family. It further attracts immune cells from the blood and the
94 interstitial space into the lung to limit and clear viral infection.
95 To delineate early tissue resident antiviral responses from those after immune cell
96 infiltration, we turned to the mPCLS model (**Fig 1A**). Brightfield microscopy confirmed the
97 maintenance of typical lung tissue architecture after tissue slicing (**Fig 1B**). mPCLS were
98 cultured for several days without signs of tissue disintegration (**Fig. S1**). The immune cell
99 compartment of mPCLS was predominantly characterized by naïve CD4 T cells and B cells in
100 the lymphoid panel (**Fig. 1C, gating strategy in Fig. S2A**) and monocytes (classical and non-

101 classical) in the myeloid panel (**Fig. 1D, gating strategy in Fig. S2B**). As compared to published
102 in vivo data[6], mPCLS show a slightly higher proportion of B lymphocytes *vs.* T lymphocyte, and
103 a generally lower representation of myeloid cells, suggesting a that the latter might be
104 partially excluded in the process of PCLS preparation.
105 The porous nature of this *ex vivo* model permitted IAV infection with a clinically relevant H1N1
106 strain influenza A/Netherlands/602/2009 (H1N1) throughout the tissue as demonstrated by
107 specific RNAscope staining of vRNA in mid-sections 48h post infection (**Fig. 1E**). We did
108 however observe a preference for infection in larger airways. A similar distribution of vRNA
109 signal was found in *in vivo* infected lung tissue 48h post infection (**Fig. 1F**). In line with this
110 viral titers *ex vivo* and *in vivo* reached comparable levels 48h post infection (**Fig 1G and H**).
111 Using a bulk RNAseq approach we compared transcriptional responses in IAV infected
112 lung tissue *in vivo* and *ex vivo*. Not surprisingly the PCA separated host responses clearly
113 between the two models (along PC1), while the IAV induced parallel shift of the global
114 transcriptome along PC2 in the two systems, which was less prominent especially in the *ex*
115 *vivo* model (**Fig. 2A**). Accordingly, we found substantially more differentially regulated genes
116 (DEG) *in vivo* than in mPCLS (**Fig. 2B-D**). Approximately 20% of the upregulated protein coding
117 DEG were classified as "immune system" related in the Reactome database[7] (**Fig. 2B**).
118 Notably, IAV induced DEG in mPCLS were largely found upregulated *in vivo* (**Fig. 2B**). The two
119 gene sets correlated with a R^2: 0.5 (**Fig. 2E**). An analysis of transcription factor binding sites in
120 promoters of upregulated genes in mPCLS indicated that IRF3 and STAT2 are mostly
121 responsible to drive the *ex vivo* response, while *in vivo* NFκB, STAT5B, NOD2 and IRF3 were
122 the most significantly enriched transcription factors (**Fig. S3A and S3B**)[8-10]. Comparative
123 Reactome analysis of mPCLS and *in vivo* mouse responses to IAV revealed a strong enrichment
124 in immune system including cytokine signaling, innate and adaptive immunity in both models

125 (**Fig. 2F**). While for mPCLS, the response was restricted to immune system activation, we
126 found *in vivo* additionally an enrichment in hemostasis, extracellular matrix organization and
127 programmed cell death among the upregulated DEG (**Fig. S3C-E**).

128 A common denominator of the antiviral response in human and murine hosts is the
129 interferon response[11]. *Ex vivo* type I and III interferon genes were generally upregulated to a
130 much lower extend than *in vivo*, with IFNB1 being the most highly induced type I interferon
131 gene (**Fig. 2G**). Accordingly, we found upregulation of typical ISGs like MX1, OAS1, or IFIT1
132 ((**Fig. 2G**) amongst others). Notably, mPCLS were completely devoid of a type II interferon
133 response (**Fig. 2G**). Accordingly, ICAM1 an experimentally confirmed type II IFN dependent
134 gene[12] was not upregulated in mPCLS after IAV challenge but type I/type III dependent genes
135 were. IFNγ is almost exclusively produced by lymphoid cells (NK, NKT, effector/memory $CD4^+$,
136 $CD8^+$ and γδ T lymphocytes). These cells were largely absent in mPCLS (**Fig. 1C**) possibly
137 explaining the lack of IFNγ in response to IAV infection.

138 Both our PCLS donor mice and the *in vivo* infected animals were immunologically naïve
139 to IAV infection, explaining the lack of tissue resident memory cells. To simulate tissue
140 responses of immune-experienced mice we generated mPCLS from IAV
141 (A/Netherlands/602/2009 H1N1) preinfected mice one month after primoinfection (**Fig. 3A**)
142 and challenged these immune experienced mPCLS with the same virus strain *ex vivo*. The
143 presence of memory T lymphocytes was confirmed by FACS (**Fig 3B and gating strategy in Fig**
144 **S4**). Viral replication was reduced in *ex vivo* tissues from IAV primed mice as confirmed by
145 qPCR for vRNA and by titration of viral supernatants (**Fig. 3C and 3D**). Surprisingly, this did
146 however not result in a generally heightened transcriptional response in IAV primed murine
147 lung tissues *ex vivo* as assessed by targeted qRT-PCR (**Fig. 3E**). Our data hence suggest an
148 increase in viral defense with improved control of viral replication one month after priming,

149 which does not generally depend on an upregulation of innate immune genes, nor seems to
150 promote it upon *ex vivo* reinfection of tissues.
151 In average a human is exposed every 5-10 years to a new influenza virus[13]. These repeated
152 infections lead to an accumulation of tissue resident memory T cells in adults. In elderly
153 influenza specific $_{trm}$T-cells decline with advanced age in lung tissue, which could in part
154 contribute to the reduced antiviral response[14]. Since elderly form a major population at risk
155 for severe IAV infection, we asked if PCLS from an immune experienced elderly human donor
156 would provide a more realistic model of tissue resident immune responses against IAV.
157 PCLS were cut from histologically healthy bystander tissue of tumor resections (for patient
158 cohort data **see Table S1**) and maintained typical 3D architecture of human lung tissue (**Fig.
159 4A**). Notably, airspaces were much larger than those found in mPCLS (**Fig. 1B**). *Ex vivo* hPCLS
160 were cultured for several days without signs of cell death comparable to mPCLS (**Fig. S1**). In
161 contrast to murine tissues T lymphocytes were the dominant lymphoid cell population in
162 hPCLS among these more than 50% effector memory CD4 and CD8 T cells (**Fig. 4B and gating
163 strategy in Fig. S5A**). Additionally, we found low percentages of NK and NKT cells, absent in
164 *ex vivo* mouse tissues. In the myeloid panel, monocytic myeloid derived suppressor cells [15]
165 and neutrophils were dominant (**Fig. 4C and gating strategy in Fig. S5B**).
166 As for mPCLS, IAV penetrated the entire tissue (**Fig 4D**) and resulted in robust viral titers 48hpi
167 (**Fig. 4E**). We found little donor to donor variation in the replication data, despite using tissues
168 from different anatomical locations of the lung and diverse underlying disease states (**Table
169 S1**), supporting the robustness of this model system for microbiological research. The PCA
170 clearly separated mock treated from IAV infected hPCLS. This is similar to data obtained from
171 an influenza virus RNA positive lung autopsie tissue from a patient who died shortly after an
172 influenza B virus diagnosis when compared to freshly isolated healthy lung tissue material

173 (**Fig. 5A**). In contrast to the mouse model, comparable numbers of DEG were upregulated in
174 hPCLS and human *in vivo* infected lung tissue. However, at protein coding gene level we found
175 only an small overlap of the upregulated DEG of hPCLS with the *in vivo* tissues (**Fig. 5B-C**). This
176 could be the consequence of a number of confounding effects: comparison of non-isogenic
177 hosts, comparison of an influenza A virus vs an influenza B virus infection, different
178 sequencing protocols (standard illumina RNAseq *vs.* exon enrichment for *in vivo*) and most
179 importantly, differences in the time point post infection. Nevertheless, the reactome analysis
180 provided however substantial overlap in upregulated gene modules related to innate immune
181 response, cytokine signaling and DNA replication, the latter being absent in murine samples
182 (**Fig. 5D and E**). On gene level the intersection of upregulated genes contained known ISGs
183 like (MX2, IFI6, IFIT1, IFIT5, IFIT3, IFI27, IRF27, IRF9, ISG15, IFITM1) were found. IAV infection
184 robustly induced type I, II and III interferons in hPCLS. Upregulation of IFNγ and IFNγ-induced
185 genes after IAV infection (**Fig. 5F**) is of interest in this model since it confirms the activation
186 and functionality of tissue resident lymphoid cells.
187 Next we were interested in testing the specificity of the transcriptomic response of hPCLS to
188 a viral infection. Using a bacterial challenge with *S. pneumoniae* (serotype 3) we expected a
189 distinct host response. As for the viral infection, bacteria penetrated the tissue to the center
190 section **(Fig. 6A**). 24h post infection with *S. pneumoniae* we observed a substantial increase
191 in bacterial titers associated with the lung tissue (**Fig. 6B**). The host response to Spn infection
192 was showed a higher donor variation and was generally less pronounced as for the viral
193 challenge (**Fig. 6C**), with patient 1 not responding to the bacterial challenge despite robust
194 bacterial replication. Since the same patient tissue reacted well to viral challenge (**Fig. 5**), we
195 conclude, this is a antigen specific effect. In contrast to the IAV response the antibacterial
196 host profile was however largely characterized by proinflammatory marker genes (e.g. IL1A

197 IL1B, TNF, IL6, IL17A) and interleukin signaling in the Reactome analysis (**Fig. 6D-F**). Lastly, we
198 tested cell-to-cell communication in the human *ex vivo* model by blocking IL-1β signaling with
199 a specific antibody. We compared the expression of IL-1β dependent genes after challenge
200 with Spn in hPCLS. Without affecting the bacterial replication (**Fig. 6G**), the blocking of IL-1β
201 signaling reduced the respective antimicrobial tissue response (**Fig. 6H**), confirming a robust
202 cell-to-cell communication in this complex *ex vivo* model.
203

204 **Discussion**

205 While primary respiratory tract epithelial cells have been shown superior to immortalized
206 lung epithelial cells with regards to antiviral responses[16], they are li Human lung-on-a-chip
207 models, lung organoids or stratified airway epithelial cells (often used in air liquid interface)
208 are mostly limited to the contribution of epithelial cells to lung infection biology. The PCLS
209 model gains rapidly importance in biomedical studies targeting lung pathologies and
210 pharmacological testing. mPCLS and hPCLS have been used to study the pathophysiology of
211 inflammatory lung diseases[17,18] and to test their response to disease relevant
212 proinflammatory stimuli[19]. In respiratory infectious disease research animal PCLS and hPCLS
213 gain importance, e.g., to assess the action of antimicrobials in a relevant organ context [20,21].
214 Others used PCLS models before to assess the innate immune response to viral challenge[22-24]
215 or to colonization with different mixes of commensal bacteria (mPCLS)[25]. Two recent studies
216 investigated viral replication and antiviral host responses in hPCLS by single cell RNAseq from
217 a single human donor[26,27]. *Ex vivo* culture lung tissue from COPD patients with terminal lung
218 emphysema was used to characterize early antiviral and antibacterial responses, 24h after
219 IAV, *Pseudomonas aeruginosa* or *Mycobacterium tuberculosis* (BCG) challenge, by scRNAseq
220 and bulk RNAseq[27]. Importantly, the authors noted a high donor dependent variation in host

221 responses. They further stated that the pre-inflamed state of these tissues might not be fully
222 representative of the antimicrobial response in healthy lung tissue. This could explain why
223 only a limited number of IAV upregulated genes were found as compared to our study. We
224 provide here comprehensive transcriptome data in human and murine ex vivo tissue
225 compared to *in vivo* host responses and complement these findings with a detailed
226 characterization of the cellular composition of the two PCLS models. While not surprising we
227 show a clear contribution of the tissue resident memory cells to human host responses
228 against IAV infection *ex vivo*. As for laboratory mice derived PCLS, the biological differences
229 to hPCLS in responsiveness to microbial infection stem likely from different genetics,
230 metabolism, microbiome and baseline immune status. The last point is of particular interest
231 when studying infectious agents since many in vivo studies rely on immunologically naïve
232 animals. Our data indicate that mPCLS from naïve mice rather poorly respond to IAV infection
233 as compared to *in vivo* infections or hPCLS. In part the lack of infiltrating immune cells into
234 the PCLS model explains these differences, but also the absence of tissue resident immune
235 cells. Beyond this, especially infiltrating monocytes and neutrophils are contributing
236 substantially to the cytokine response and eventually immune pathology observed during a
237 severe viral pneumonia[28]. Hence proinflammatory signaling was not faithfully reproduced
238 especially in the naïve murine *ex vivo* model. Exogenous addition of monocytes from blood or
239 bone marrow might be a strategy to compensate for the absence of a connection to the
240 supply with blood derived immune cells to overcome the limited antiviral response. PCLS from
241 animals with multiple IAV encounters could serve as a better model to mimic the immune
242 history observed in human patients, who on average undergo an IAV infection every 5-10
243 years[13]. Surprisingly, the innate antiviral host response did not differ in these animals. We
244 found for example no increased expression of IFNγ, suggesting that tissue resident T-

245 lymphocytes do not contribute to the increased protection. Considering the high number of
246 B lymphocytes in mPCLS, we suspect an antibody mediated partial neutralization of viral
247 infection. Globally, we observed specific antiviral and antibacterial responses in both PCLS
248 systems, suggesting a clear distinction between the two types of pathogens. It must be noted
249 that the timing (48h IAV *vs* 24h Spn) could in part explain these differences. Notably, a recent
250 report indicated that PCLS undergo a spike of innate immune and inflammatory gene
251 induction on the day of cutting which wanes within 24h[29]. It is unclear how this mechanic
252 induction of the innate immune response affects a subsequent challenge with viral or
253 bacterial pathogens. The lack of IFNγ induction by IAV infection in mPCLS was suggesting that
254 the early antiviral response in *ex vivo* tissues naïve animals relies purely on a type I interferon
255 responses. In contrast antibacterial/proinflammatory signaling after Spn challenge was
256 readily detectable in mPCLS but less in hPCLS. This also suggests that mPCLS are not generally
257 unresponsive to microbial exposure. In fact, an important contributor to the antibacterial host
258 responses in mice is age. PCLS from aged mice display a stronger inflammatory reaction to
259 bacterial PAMP than tissues from young animals[30]. In hPCLS from aged patients, we detected
260 a distinct proinflammatory host response after Spn colonization, as compared to the antiviral
261 response. Globally this response was less pronounced as the antiviral response despite robust
262 bacterial replication. In fact, hPCLS from one human patient did not upregulate innate
263 immune response genes after Spn challenge, but at the same time responded well to IAV,
264 which suggest potentially an individual response based on previous exposure to pneumococci
265 and potentially depending on patient specific subsets of tissue resident immune cells.
266 Alternatively, tolerance mechanisms towards this common pathobiont in the upper
267 respiratory tract of humans might play a role in dampening the antibacterial response. This
268 could indicate that hPCLS could reflect the individual exposure history of a given patient and

269 hence be used to study the basic cellular response in lung tissue based on immune history
270 shaped cell composition. Such a tool would be useful to predict innate responses in lung tissue
271 of different age groups, e.g., to novel influenza viruses, where preexisting immunity can play
272 an important role to prevent mortality in critical target groups as reported for the 2009 H1N1
273 pandemic[31]. IFI27 for example was previously identified as marker for IFN responses in
274 peripheral immune cells (monocytes and conventional DC) of influenza virus infected human
275 patients[32], suggesting that some of these immune cells could reside in hPCLS. The shortage of
276 human biopsy/autopsy material collected early during an IAV infection makes it difficult to
277 conclusively answer these questions. On a more applied note, we think that hPCLS could be
278 used to test antivirals or anti-inflammatory drugs in a realistic environment with additional
279 viral restriction provided by the tissue resident immune cells and with an architecture and
280 accessibility reflecting that of the native tissue.
281

282 **Material and Methods**

283 **Ethics**

284 Human tissue was obtained from the thorax surgery of the university hospital Geneva (HUG)
285 and its use was approved under the license 2022-01942 by the CCER. Written patient consent
286 was provided. Animal experiments were approved by the cantonal authorities and
287 institutional animal welfare board under license number: GE216).

288 ***PCLS generation***

289 mPCLS: C57BL/6J mice (female, 7–10 weeks of age) were purchased from Charles River
290 Laboratories (France) and housed at least 7 days under SPF conditions with a strict 12h/12h
291 light/dark cycle and food and water at libitum. Animals were euthanized by intraperitoneal
292 injection of pentobarbital (150µg/g, Esconarkon®, Streuli Pharma, Uznach, Swtizerland) when

293 experimental or humane endpoints were reached. To collect lung tissues, the abdominal
294 cavity and the thoracic cage were opened surgically. The inferior vena cava was nicked, and
295 lung lavage was performed by PBS 1X injection into the heart right vena. Next, a catheter
296 (22G) was inserted in the trachea to perfuse the lungs with 2% low-melting-point agarose
297 warmed to 37°C (Sigma-Aldrich, A9414, diluted in DMEM/Ham's F12, Gibco). The mouse was
298 cooled at 4°C for 10 min, then the lung was excised and incubated 30 min at 4°C to let the
299 agarose solidified. The lobes were dissociated and murine PCLS (250µm thickness) were cut
300 with a Krumdieck tissue slicer (Alabama R&D, USA, MD600).
301 hPCLS: The use of human tissue was approved by the cantonal ethics committee of Geneva
302 (CCER, project number 2022-01942). Lung tissues were provided by the thorax surgery unit
303 of the University Hospital Geneva (Hôpitaux Universitaires de Genève, HUG). Tumor-free
304 tissue from lung cancer resection surgeries of 22 patients were collected for this work. The
305 average age was 67.4 (±10.7) years, 12 were females and 10 males. Concerning smoking
306 habits: 8 were active, 7 formers smokers, 3 non-smokers, and 4 were without information.
307 Location of the resected tissue was in lower left lobe (3), lower right (2), upper left (6), upper
308 right (8), middle right (3). Individual underlying disease state and medication are indicated in
309 **Table S1**. The lung segment was washed with PBS 1X and perfused with 2% low-meting-point
310 agarose thanks to catheters (22G). The solidification was allowed by 1h30 at 4°C on ice. Using
311 a coring press (Alabama R&D, USA MD500), tissue cylinders of 8mm diameter were generated
312 and transversally sliced into PCLS as described for mPCLS. PCLS were maintained in 500µL
313 DMEM/Ham's F12 (Gibco, supplemented with 100 U/mL penicillin and 100 µg/mL
314 streptomycin (Sigma-Aldrich, P0781) without FCS) in 24-wells plate at 37°C, 5% CO2. The
315 medium was changed 2 hours after cutting to remove the agarose, experiments were
316 performed the day after the cutting to allow tissue recovering and agarose dissolution. Tissue

317 integrity was confirmed with a brightfield microscope (Evos microscope system, Thermo
318 Fisher).

319 ***Bacteria***

320 Spn (ATCC: (Klein) Chester 6303, serotype 3) was grown in Trypticase Soy Broth (Oxoid, UK,
321 BO0369M) at 37°C with 5% CO_2 in static culture up to 0.4 optical density (OD600 nm). PCLS
322 infection was performed using 10^3CFU per well in the PCLS culture medium at 37°C, 5% CO_2.
323 The inoculum was removed after 4h incubation, PCLS were washed two times with PBS 1X
324 and fresh culture medium was added. The infection was stopped 24h post-inoculation.
325 Supernatants and tissues were collected. Tissues were homogenized with a BeadBlaster
326 homogenizer (Benchmark, D2400) using 1.4mm ceramic beads to determine bacterial titers
327 (Omni International, 19627). Serial dilutions were spotted on Trypticase Soy agar plates with
328 5% sheep blood (BioMerieux, M1006) at 37˚C with 5% CO2.

329 ***Viruses***

330 A/Netherlands/602/2009 (H1N1)[33] was kindly provided by Dr. Florian Krammer (Icahn School
331 of Medicine at Mount Sinai, New York, NY, USA). PCLS were infected with 10^5 PFU in 200µl of
332 PCLS medium per well. After 50 min of viral adsorption at 37°C, PCLS were washed with PBS
333 1X and incubated in fresh culture medium. Supernatants were collected at the indicated times
334 post infection and viral titers were determined by plaque assay in MDCK cells (Madin-Darby
335 canine kidney, ATCC).

336 ***Plaque assays***

337 MDCK cells were grown in DMEM (Dulbecco's Modified Eagle Medium, Gibco) supplemented
338 with 10% (vol/vol) heat-inactivated fetal bovine serum (Gibco) and 100 U/mL penicillin and
339 100 µg/mL streptomycin (Sigma-Aldrich, P0781). Cells (6-well plate format, 1,5 x 10^6
340 cells/well) were infected with 10-fold serial dilutions in PBS 1X 0,2% BSA of the virus for 50

341 min at 37°C. Supernatants were replaced by fresh overlay medium supplemented with 1
342 mg/mL of N-tosyl-L-phenylalanine chloromethyl ketone (TPCK)-treated trypsin (Sigma) and
343 0,6% purified agar (Oxoid) and plates were incubated at 37°C 5% CO_2. After 48 h, cells were
344 fixed for 1 h at RT with 4% paraformaldehyde (PFA) and the overlays were removed. Cells
345 were stained using a solution of 16% Methanol and crystal violet and plaques were counted
346 visually.

347 ***In vivo infection***

348 For inoculation with IAV, mice were injected intraperitoneally with a mix of ketamine/xylazine
349 (100 mg/kg and 5 mg/kg, respectively) in 200 µl of sterile PBS. Upon reaching deep anesthesia,
350 mice were inoculated with 40 µl of PBS or virus (10^4 PFU) via the intranasal route. Lungs were
351 collected after 24h and 48 hpi for IAV.

352 ***RNA extraction & RT-qPCR***

353 Tissue was stored at -80°C in RNA protect Tissue reagent (Qiagen, 76104, Germany). PCLS
354 were disrupted in the lysis buffer from the kit with 1.4mm ceramic beads (Omni International,
355 19627) using a BeadBlaster homogenizer (Benchmark, D2400). Then, RNA extraction was
356 performed with the NucleoSpin RNA XS kit (Macherey-Nagel, 740902), following the
357 manufacturer's instructions. Elution was done in 30µl of water. RNA concentration was
358 estimated by Nanodrop. 250 ng were used for reverse-transcription using the MMLV-RT
359 (Invitrogen, 28025013). Gene expression was assessed by quantitative PCR using 2X KAPA
360 SYBR FAST qPCR Master Mix-Universal (KAPA Biosystems, USA) and 10 µM of forward and
361 reverse primers (**Table S2**). PCR was realized with CFX Connect Real-Time PCR detection
362 system (Biorad) following this thermal cycling protocol: an initial denaturation step at 95 °C
363 for 10 min, followed by 45 cycles of denaturation at 95 °C for 15 s, annealing/extension at
364 61.5 °C for 60 s, with a final melting curve step from 60 to 95 °C with 0.5 °C increment. The

365 relative gene expression was calculated with the ΔΔCt method, using *hprt* (murine tissue) or
366 18s-rRNA (human tissue) genes for normalization.
367 For all lungs from mice or unprocessed lung biopsies from human, total RNA was extracted
368 using TRIzol (Ambion, Life technologies) following manufacturer's instructions.

369 ***Lactate dehydrogenase (LDH) assay***

370 To determine global cell suffering, LDH release was quantified daily into the PCLS supernatant
371 using the colorimetric test CYQUANT ™ LDH cytotoxicity assay kit (Invitrogen, C20300),
372 according to the manufacturer's recommendations.

373 ***RNAscope***

374 PCLS from mice and human were collected under sterile conditions, fixed in PBS 1X -
375 paraformaldehyde 4% solution overnight at 4°C and embedded in paraffin and sliced using a
376 standard microtome (5 µM thickness). *In situ* detection of *Streptococcus pneumoniae*
377 (RNAscope® Probe - B- S. pneumoniae -SPN23F12870-C2, accession number: FM211187.1,
378 nucleotides: 2-753) and IAV (RNAscope® Probe V - Influenza A - H1N1 – segment 5 – NP - O8
379 -C1, accession number: CY176945.1) was performed using the RNAscope 2.5 HD Assay - RED
380 (Advanced Cell Diagnostics) according to the manufacturer's protocol. Briefly, tissue slices
381 were deparaffinized by 1h incubation at 60°C followed by four rounds in 100% xylol and four
382 rounds in 100 % ethanol solutions. An incubation with hydrogen peroxide was performed for
383 10 min and target retrieval was achieved by incubating the slides with RNAscope 1x Target
384 Retrieval Reagent for 45 min at 95°C. Tissue was permeabilized using RNAscope protease plus
385 for 30 min (Advanced Cell Diagnostics). Probe hybridization was performed with a specific
386 RNA probe for IAV or Spn for 2 h at 40°C. Signal amplification was achieved by incubating the
387 tissues at 40°C with AMP solutions provided by the kit. Cyanine 3 and cyanine 5 were used as
388 fluorophores respectively for IAV and Spn. Slides were counterstained with Prolong Diamond

389 Antifade Mountant with DAPI (Invitrogen, P36962). Slides were visualized under Nikon A1r
390 spectral microscope under a x10/20 objective and processed using Zen Software.

391 ***Transcriptomic analysis***

392 RNA was extracted as described before at the replication peak of each pathogen (48h for IAV,
393 24h for Spn). RNAseq (30 million reads per sample (triplicates for each murine condition, five
394 patients samplings for hPCLS) was performed at the iGE3 Genomics Platform at the University.
395 Analysis of these data was realized with the help of the Bioinformatics Support Platform
396 (UNIGE). Libraries were prepared with the Illumina TruSeqHT Stranded mRNA protocol for
397 PCLS and mouse in vivo lungs and with RNA exome-seq for human in vivo autopsy samples
398 and corresponding control. The sequencing was done on Illumina NovaSeq 6000 sequencer.
399 Sequenced reads were mapped with HISAT2 aligner either to the mouse genome GRCm39
400 (source: ensembl 110) or to the human genome GRCh38.p14 (source: ensembl 110). Read-
401 count quantification was extracted with the method summarizeOverlaps() from R package
402 GenomicAlignments. The code and softwares used in the analysis were packaged into a
403 docker container made publicly available at https://github.com/BioinfoSupport/ngs
404 (container), https://github.com/ BioinfoSupport/rnaseq (mapping and quantification
405 pipeline), and https://github.com/BioinfoSupport/genomes (for HISAT2 indexed genomes).
406 Normalization, differential gene expression analysis, and data visualization were conducted
407 with the R programming language. Package DESeq2 was used to asset the statistical
408 significance of differential gene expressions. More specifically, we conducted 4 independent
409 DESeq2 analyses to take into consideration samples pairing: A) one with 6 unpaired samples
410 of the mouse in vivo conditions (mIV_mock, mIV_IAV); B) another with the 6 paired-samples
411 of the mouse PCLS conditions (mPCLS_mock, mPCLS_IAV); C) a last with 15 paired samples of
412 the human PCLS conditions (hPCLS_mock, hPCLS_Spn, hPCLS_IAV); D) one with 6 unpaired

413 samples of the human in vivo conditions (hIV_mock, hIV_Influenza). The details of the
414 samples used in each set is given in **Table S3** "RNA-seq Samples description". Pathway
415 enrichment analysis was done under the R programming language with hypergeometric tests
416 against Reactome.org database. Transcription factor enrichment analysis was realized using
417 EnrichR[8-10].

418 ***Flow cytometry***

419 One day after slicing, 14 PCLS per condition were washed with cold PBS 1X and pooled
420 together. Cell dissociation was performed for 45 minutes at 37°C (aggitation) with PBS +5%
421 FBS with 0.5 mg/mL Collagenase D and 0.1mg/mL DNaseI. Cells were centrifugated 5 min at
422 300g. Red blood cell lysis was performed with ACK buffer for 4 minutes at RT. The reaction
423 was stopped with RPMI 10% FBS and cells were spined and washed in PBS.
424 Cells were stained 15 min at RT with Fixable Viability Dye (Invitrogen, 1:1000 in PBS 1X) and
425 FC blocking was performed with 0.25µg of TruStain FcX PLUS (Biolegend) in 100µL of MACS
426 before staining. Cells were then stained 15 min on ice with surface markers antibodies
427 resuspended in MACS buffer (PBS-0.5% BSA- 2mM EDTA) according to the panel. Antibodies
428 references are indicated in **Table S4**. Cells were fixed with 200 µL of IC Fixation Buffer
429 (Thermofisher) for 30 min at RT. Samples were centrifugated at 450g at RT for 5 min. Cells
430 were resuspended in an appropriate volume of MACS buffer and the samples were run on
431 LSRII Fortessa instrument (BD Biosciences).

432 ***IL-1β blocking experiment in hPCLS.***

433 hPCLS were infected with 10^3 CFU of Spn, after 4h of attachment, PCLS were washed 2 times
434 with PBS 1X and culture medium containing 10µg/ml antibody anti-ILβ (R&D Systems,
435 MAB601, clone 2805) was added. Tissues and supernatants were collected 24hpi. Stastistical
436 analysis was

437 ***Statistical analysis***

438 Statistical analysis was performed using GraphPad Prism 9 or R and statistical tests applied as
439 well as the number of biological and technical repeats are indicated in each respective figure
440 legend.

441 **Acknowledgments:**

442 Our work was supported by a generous donor, advised by CARIGEST SA and the Fondation
443 privée des HUG. We are extremely grateful for the generous donation of tissue samples by
444 HUG patients in support of our research and for the professional collaboration with the
445 surgical team of the HUG providing this. We would further like to thank the animal care takers
446 at the CMU for their daily support as well as the core facilities for iGE3 Genomics, Bioimaging,
447 Histology and Cytometry. We are grateful for the insightful advise by Prof. Dorothee Viemann
448 and Prof Benjamin G. Hale.

449

450 **Conflicts of interest**

451 The authors declare that they have no conflict of interest.

452

453 **References**

454 1 The top 10 causes auf death. *WHO fact sheets* (2024).
455 2 Travaglini, K. J. *et al.* A molecular cell atlas of the human lung from single-cell RNA
456 sequencing. *Nature* **587**, 619-625 (2020). https://doi.org:10.1038/s41586-020-2922-4
457 3 Parrish, A. R., Gandolfi, A. J. & Brendel, K. Precision-cut tissue slices: applications in
458 pharmacology and toxicology. *Life Sci* **57**, 1887-1901 (1995).
459 https://doi.org:10.1016/0024-3205(95)02176-j
460 4 Fisher, R. L. *et al.* The use of human lung slices in toxicology. *Hum Exp Toxicol* **13**,
461 466-471 (1994). https://doi.org:10.1177/096032719401300703
462 5 Koziol-White, C., Gebski, E., Cao, G. & Panettieri, R. A., Jr. Precision cut lung slices:
463 an integrated ex vivo model for studying lung physiology, pharmacology, disease
464 pathogenesis and drug discovery. *Respir Res* **25**, 231 (2024).
465 https://doi.org:10.1186/s12931-024-02855-6

466 6 Yu, Y. R. *et al.* A Protocol for the Comprehensive Flow Cytometric Analysis of
467 Immune Cells in Normal and Inflamed Murine Non-Lymphoid Tissues. *PLoS One* **11**,
468 e0150606 (2016). https://doi.org:10.1371/journal.pone.0150606
469 7 Milacic, M. *et al.* The Reactome Pathway Knowledgebase 2024. *Nucleic Acids Res* **52**,
470 D672-D678 (2024). https://doi.org:10.1093/nar/gkad1025
471 8 Chen, E. Y. *et al.* Enrichr: interactive and collaborative HTML5 gene list enrichment
472 analysis tool. *BMC Bioinformatics* **14**, 128 (2013). https://doi.org:10.1186/1471-2105-
473 14-128
474 9 Kuleshov, M. V. *et al.* Enrichr: a comprehensive gene set enrichment analysis web
475 server 2016 update. *Nucleic Acids Res* **44**, W90-97 (2016).
476 https://doi.org:10.1093/nar/gkw377
477 10 Xie, Z. *et al.* Gene Set Knowledge Discovery with Enrichr. *Curr Protoc* **1**, e90 (2021).
478 https://doi.org:10.1002/cpz1.90
479 11 Meyts, I. & Casanova, J. L. Viral infections in humans and mice with genetic
480 deficiencies of the type I IFN response pathway. *Eur J Immunol* **51**, 1039-1061 (2021).
481 https://doi.org:10.1002/eji.202048793
482 12 Der, S. D., Zhou, A., Williams, B. R. & Silverman, R. H. Identification of genes
483 differentially regulated by interferon alpha, beta, or gamma using oligonucleotide
484 arrays. *Proc Natl Acad Sci U S A* **95**, 15623-15628 (1998).
485 https://doi.org:10.1073/pnas.95.26.15623
486 13 Kucharski, A. J. *et al.* Estimating the life course of influenza A(H3N2) antibody
487 responses from cross-sectional data. *PLoS Biol* **13**, e1002082 (2015).
488 https://doi.org:10.1371/journal.pbio.1002082
489 14 Nguyen, T. H. *et al.* Influenza, but not SARS-CoV-2, infection induces a rapid
490 interferon response that wanes with age and diminished tissue-resident memory CD8(+)
491 T cells. *Clin Transl Immunology* **10**, e1242 (2021). https://doi.org:10.1002/cti2.1242
492 15 Bronte, V. *et al.* Recommendations for myeloid-derived suppressor cell nomenclature
493 and characterization standards. *Nat Commun* **7**, 12150 (2016).
494 https://doi.org:10.1038/ncomms12150
495 16 Bertrams, W. *et al.* Transcriptomic comparison of primary human lung cells with lung
496 tissue samples and the human A549 lung cell line highlights cell type specific responses
497 during infections with influenza A virus. *Sci Rep* **12**, 20608 (2022).
498 https://doi.org:10.1038/s41598-022-24792-4
499 17 Boucher, M. *et al.* High throughput screening of airway constriction in mouse lung
500 slices. *Sci Rep* **14**, 20133 (2024). https://doi.org:10.1038/s41598-024-71170-3
501 18 Kortekaas, R. K. *et al.* The disruptive effects of COPD exacerbation-associated factors
502 on epithelial repair responses. *Front Immunol* **15**, 1346491 (2024).
503 https://doi.org:10.3389/fimmu.2024.1346491
504 19 Stephenson, K. E. *et al.* The IL-33:ST2 axis is unlikely to play a central fibrogenic role
505 in idiopathic pulmonary fibrosis. *Respir Res* **24**, 89 (2023).
506 https://doi.org:10.1186/s12931-023-02334-4
507 20 Mazel-Sanchez, B. *et al.* Influenza A virus exploits transferrin receptor recycling to
508 enter host cells. *Proc Natl Acad Sci U S A* **120**, e2214936120 (2023).
509 https://doi.org:10.1073/pnas.2214936120
510 21 Diesendorf, V. *et al.* Drug-induced phospholipidosis is not correlated with the
511 inhibition of SARS-CoV-2 - inhibition of SARS-CoV-2 is cell line-specific. *Front Cell*
512 *Infect Microbiol* **13**, 1100028 (2023). https://doi.org:10.3389/fcimb.2023.1100028
513 22 Michalaki, C., Dean, C. & Johansson, C. The Use of Precision-Cut Lung Slices for
514 Studying Innate Immunity to Viral Infections. *Curr Protoc* **2**, e505 (2022).
515 https://doi.org:10.1002/cpz1.505

516 23 Pickles, R. J., Chen, G. & Randell, S. H. Enhanced susceptibility of pediatric airway
517 epithelium to respiratory syncytial virus infection. *J Clin Invest* **134** (2024).
518 https://doi.org:10.1172/JCI185689
519 24 Brugger, M. *et al.* Aging shapes infection profiles of influenza A virus and SARS-CoV-
520 2 in human precision-cut lung slices. *Respir Res* **26**, 112 (2025).
521 https://doi.org:10.1186/s12931-025-03190-0
522 25 Tony-Odigie, A., Wilke, L., Boutin, S., Dalpke, A. H. & Yi, B. Commensal Bacteria in
523 the Cystic Fibrosis Airway Microbiome Reduce P. aeruginosa Induced Inflammation.
524 *Front Cell Infect Microbiol* **12**, 824101 (2022).
525 https://doi.org:10.3389/fcimb.2022.824101
526 26 Crue, T. *et al.* Single cell RNA-sequencing of human precision-cut lung slices: A novel
527 approach to study the effect of vaping and viral infection on lung health. *Innate Immun*
528 **29**, 61-70 (2023). https://doi.org:10.1177/17534259231181029
529 27 Sohail, A. *et al.* Differential transcriptomic host responses in the early phase of viral
530 and bacterial infections in human lung tissue explants ex vivo. *Respir Res* **25**, 369
531 (2024). https://doi.org:10.1186/s12931-024-02988-8
532 28 Seo, S. U. *et al.* Type I interferon signaling regulates Ly6C(hi) monocytes and
533 neutrophils during acute viral pneumonia in mice. *PLoS Pathog* **7**, e1001304 (2011).
534 https://doi.org:10.1371/journal.ppat.1001304
535 29 Preuss, E. B. *et al.* The Challenge of Long-Term Cultivation of Human Precision-Cut
536 Lung Slices. *Am J Pathol* **192**, 239-253 (2022).
537 https://doi.org:10.1016/j.ajpath.2021.10.020
538 30 Diaz-Nicieza, C., Sahyoun, L., Michalaki, C., Johansson, C. & Culley, F. J. Ageing
539 results in an exacerbated inflammatory response to LPS by resident lung cells. *Immun*
540 *Ageing* **21**, 62 (2024). https://doi.org:10.1186/s12979-024-00467-8
541 31 Karageorgopoulos, D. E., Vouloumanou, E. K., Korbila, I. P., Kapaskelis, A. &
542 Falagas, M. E. Age distribution of cases of 2009 (H1N1) pandemic influenza in
543 comparison with seasonal influenza. *PLoS One* **6**, e21690 (2011).
544 https://doi.org:10.1371/journal.pone.0021690
545 32 Zhang, Y. *et al.* A single-cell atlas of the peripheral immune response in patients with
546 influenza A virus infection. *iScience* **26**, 108507 (2023).
547 https://doi.org:10.1016/j.isci.2023.108507
548 33 Pica, N., Langlois, R. A., Krammer, F., Margine, I. & Palese, P. NS1-truncated live
549 attenuated virus vaccine provides robust protection to aged mice from viral challenge.
550 *J Virol* **86**, 10293-10301 (2012). https://doi.org:10.1128/JVI.01131-12
551

552 **Figure legends**

553 **Figure 1: Modeling the early host response against Influenza A virus in murine PCLS.**

554 A) Schematic of PCLS generation: lungs are perfused with a low melting agarose solution to
555 preserve the 3D lung architecture. After solidification at 4°C, lungs are cored into regular
556 cylinders and processed to slicing using a microtome. PCLS are then kept in culture
557 medium at 37°C.

558 B) Brightfield picture of an untreated murine PCLS. Scale bar represents 400µm.

559 C-D) Untreated PCLS were enzymatically digested one day after slicing to characterize
560 baseline composition of lymphoid (C) and myeloid (D) immune cells. Results are presented in
561 % of total lymphoid population and in % of total myeloid population (N=3). **Lymphoid cells**:
562 LB: lymphocytes B, gdLT: γδ T lymphocytes, NK: natural killer cells, NKT: natural killer T cells,
563 LT: lymphocyte T, n: naïve, cm: central memory, em: effector memory. **Myeloid cells**: AMs:
564 Alveolar macrophages, Neut: neutrophils, DCs: dendritic cells, ClaMs: classical monocytes,
565 PatMs: patrolling monocytes.

566 Mice and mPCLS were respectively infected with $10^4/10^5$ PFU of IAV
567 (A/Netherlands/602/2009/H1N1) for 24 or 48h.

568 E-F) In situ RNA hybridization of viral nucleoprotein (Cyanine 3) was used to visualize IAV at
569 48hpi in mPCLS sections (E) and in vivo in mouse lungs (F). Confocal observation was done at
570 x100 (top pictures IAV & uninfected, size bar represents 100µM) or at x200 (bottom pictures,
571 size bar represents 50µm).

572 G-H) Titers were measured by plaque-assay on mPCLS (G, N=4, duplicates) and on in vivo
573 infected lung (H, N=3) at 24 and 48hpi.

574 **Figure 2: Comparative transcriptomic analysis of the early host response to Influenza A virus**
575 **in murine lung in vivo and ex vivo**

576 Mice and mPCLS were respectively infected with $10^4/10^5$ PFU of IAV
577 (A/Netherlands/602/2009/H1N1) for 48h. Tissue was processed to bulk RNA sequencing and
578 host response was analyzed on R using Deseq2 package.

579 A) Principal component analysis illustrates the transcriptional response of mock treated
580 (blue) and IAV-infected lung tissue (orange) in vivo and in mPCLS. Arrows indicate the
581 pairs of mock and infected PCLS from the three independent experiments.

582 B) Venn diagrams of the commonly upregulated (orange) or downregulated (blue) genes in
583 mouse in vivo and mPCLS infected with IAV. The white circle indicates the genes related
584 to immune system pathways (using Reactome annotations).

585 C-D) Volcano plot showing differentially expressed genes between IAV-infected and mock
586 samples in mouse in vivo (C) and in mPCLS (D). Log2 fold-change induction is indicated in the
587 x-axis, -log10(p-adjusted) in the y-axis. Genes have been represented in: orange
588 (upregulated), blue (downregulated), grey (not significant). Genes associated to immune
589 system pathways are depicted in black.

590 E) Scatter plot comparing the genes regulated by IAV in mouse in vivo (log2 Fold Change in x-
591 axis) and in mPCLS (log2 Fold Change in y-axis). Correlation is indicated with R Pearson
592 coefficient (R=0.5, p<2.2E-16). Color legend indicates the direction for mouse in vivo/mPCLS
593 genes regulated.

594 F) Pathway enrichment analysis was conducted using hypergeometric tests against
595 Reactome.org database. -log10 (p-adjusted) is given by a color scale. Coverage percentage of
596 the pathway set is indicated by the size of the dot. Pathways are indicated with the total
597 number of genes in brackets and the number of genes significantly regulated are indicated
598 next to the dot. Significantly enriched pathways are indicated by a black circle.

599 G) Heatmap illustrates the regulation of interferon signaling genes by IAV 48hpi in mouse in
600 vivo and in mPCLS. Genes are represented by the log2 Fold Change (pink: positive log2FC,
601 blue: negative log2FC), * indicates if the gene is significantly regulated by IAV infection.

602 **Figure 3: Characterization of the innate immune response in IAV-primed mPCLS**

603 A) Mice were intranasally primed with PBS or 40pfu of A/Netherlands/602/2009/H1N1
604 (N=3, duplicates). One month later, mice were sacrificed and mPCLS were generated

605 and homologously re-infected with 10^5 pfu of IAV for 48h. Supernatants and tissues
606 were collected for titers and RNA extraction.
607 B) Flow cytometry was conducted on untreated mPCLS from PBS or IAV-primed mice.
608 Lymphoid cell population was quantified.
609 C) Viral replication was measured at 48hpi by RT-qPCR on M1 gene on IAV-infected PCLS
610 from PBS and IAV-primed mice.
611 D) Viral titers 48 hpi were measured by plaque-assay.
612 E) RT-qPCR on antiviral genes was performed 48hpi. Fold change over mock are
613 represented.

614 Statistical analysis was done with a t-test (N=3, each symbol represents one independent
615 experiment). PBS-primed mPCLS are represented in white boxes and IAV-primed mPCLS
616 in blue boxes. p-value is indicated.

617 **Figure 4: Antimicrobial host response to viral challenge in the human PCLS model**

618 A) Brightfield picture of an untreated human PCLS in culture (magnification X100, size bar
619 represents 400µM).

620 B-C) Untreated PCLS from 3 patients were enzymatically digested one day after slicing to
621 describe the baseline composition of lymphoid (B) and myeloid (C) immune cells. Results
622 are presented in % of total lymphoid population and in % of total myeloid population.
623 **Lymphoid cells:** LB: lymphocytes B, gdLT: γδ T lymphocytes, NK: natural killer cells, NKT:
624 natural killer T cells, LT: lymphocyte T, n: naïve, cm: central memory, em: effector
625 memory, emra: effector memory $CD45RA^+$. **Myeloid cells**: AMs: Alveolar macrophages,
626 OtMs: other macrophages, Neut: neutrophils, DCs: dendritic cells, ClaMs: classical
627 monocytes, NClaMs: non-classical monocytes, IntMs: Intermediate monocytes .

628 D) In situ RNA hybridization of viral nucleoprotein (Cyanine 3) was used to visualize IAV
629 at 48hpi in hPCLS sections. Magnification x200. Size bar is representing 50 µm.
630 E) hPCLS were infected with 10^5 pfu of IAV (A/Netherlands/602/2009/H1N1) for 8 days,
631 viral titers were measured daily by plaque-assay (3 patients in duplicates).

632 **Figure 5: Antimicrobial host response to viral challenge in the human PCLS model *versus* in**
633 **vivo human lungs**

634 Human PCLS from five patients were infected with 10^5 pfu of IAV
635 (A/Netherlands/602/2009/H1N1) for 48h. In parallel, lung biopsies from a naturally Influenza-
636 infected patient *in vivo* (triplicates from three different lobes) were compared to unprocessed
637 lung samples from three uninfected patients. Bulk RNA sequencing was performed on these
638 samples and analysis was conducted using Deseq2 package on R software.

639 A) Principal component analysis illustrates the global transcriptomics response of control
640 (blue) and Influenza-infected (orange) samples in human in vivo (left) and in hPCLS (right).
641 B) Venn diagrams of the commonly upregulated (orange) or downregulated (blue) genes in
642 human *in vivo* and hPCLS after influenza infection. The white circle indicates the genes
643 related to immune system pathways.
644 C) Volcano plot showing differentially expressed genes between Influenza-infected and mock
645 samples in human in vivo (left) and in hPCLS (right). Log2 fold-change induction is indicated
646 in the x-axis, -log10(p-adjusted) in the y-axis. Genes have been represented in: orange
647 (upregulated), blue (downregulated), grey (not significant). Genes associated to immune
648 system pathways are illustrated in black.
649 D) Pathway enrichment analysis was conducted using Reactome database. -log10 (p-
650 adjusted) is given by a color scale. Coverage percentage of the pathway set is indicated by
651 the size of the dot. Pathways are indicated with the total number of genes in brackets and

652 the number of genes significantly regulated are indicated next to the dot. Pathways
653 significantly enriched are surrounded by a black circle.
654 E) Heatmaps indicate the commonly up genes in human in vivo and in hPCLS after influenza
655 infection for Innate Immune System, Cytokine Signaling and DNA replication pathways.
656 Genes are ranked by the log2 Fold Change (upregulated: pink, downregulated: blue).
657 F) Heatmap of genes associated with interferon signaling. The significance of regulation by
658 IAV in human in vivo and in hPCLS is indicated by a *.

659 **Figure 6: hPCLS can reproduce a classical antibacterial response towards a bacterial**
660 **challenge**

661 Human PCLS from five patients were infected with 10^3 cfu of *Streptococcus pneumoniae* (Klein
662 Chester ATCC 6303, serotype 3) for 24h. Bioinformatic analysis was done using Deseq2 with
663 R programming.
664 A) In situ RNA hybridization of dnaA (Cyanine 5) was used to visualize *Spn* at 24hpi in hPCLS
665 sections. Magnification x100. Size bar is representing 100 µm. Mock are uninfected hPCLS.
666 B) Bacterial titers from tissue homogenates of PCLS were measured at 24hpi (N=5,
667 duplicates).
668 C) Principal component analysis illustrates the global transcriptomics response of mock
669 treated (blue) and Spn infected 24hpi (orange) hPCLS. Arrows indicate the corresponding
670 infected sample for each patient mock sample.
671 D) Volcano plot showing differentially expressed genes between Spn infected and mock
672 treated samples. Log2 fold-change induction is indicated in the x-axis, p-adjusted in the
673 y-axis. Genes have been represented in: orange (upregulated), blue (downregulated),
674 grey (not significant). Genes associated to immune system pathways are represented in
675 black.

676 E) Pathway enrichment analysis was conducted using Reactome database (hypergeometric
677 test). The top 10 pathways upregulated by *Spn* infection are shown. -log10 (p-adjusted)
678 is given by a color scale. Coverage percentage of the pathway set is indicated by the size
679 of the dot. Pathways are indicated with the total number of genes in brackets and the
680 number of genes significantly regulated are indicated next to the dot.
681 F) Heatmaps of the top 30 genes significantly upregulated (pink) and downregulated (blue)
682 by Spn in hPCLS from 5 patients. Genes are ranked by the log2 Fold Change.

683 G-H) hPCLS have been infected 24h with Spn (10^3 cfu) and co-treated with an IL-1β blocking
684 antibody (10µg/ml) (N=3, duplicates). G) Bacterial titers have been measured. H) RT-qPCR
685 has been realized on a panel of genes associated to IL-1β signaling for Spn infection.
686 Statistical significance was established with a one-way ANOVA (N=3, each symbol represents
687 one independent experiment). White boxes are the Spn-infected hPCLS, grey boxes are co-
688 treated with anti-IL-1β cocktail.

689 **Supplementary figures:**

690 **Figure S1: Viability of mPCLS and hPCLS in culture.**

691 Cell death was measured in mPCLS (in green) and hPCLS (in gray) by quantification of LDH
692 release upon 4 days post-slicing. Positive control of cell death (100%) was realized with triton
693 10X treatment (N=3, duplicates).

694 **Figure S2: Flow cytometry gating strategy to describe immune cells in murine PCLS**

695 Examplary gating strategy is shown for A) Lymphoid cell panel B) Myeloid cell panel

696 **Figure S3: Signaling activation in mouse in vivo and ex vivo 48h after IAV infection**

697 Mice and mPCLS were respectively infected with $10^4/10^5$ PFU of IAV
698 (A/Netherlands/602/2009/H1N1) for 48h. Tissue was processed to bulk RNA sequencing and
699 host response was analyzed using 'DeSeq2' package on R. Transcription factor enrichment

700 analysis was conducted using EnrichR platform for IAV host responses in mouse in vivo (A)
701 and ex vivo (B). Only transcription factors significantly enriched are indicated. Odds ratios
702 are indicated in x-axis and p-value in y-axis. Hemostasis pathway (C), Extracellular matrix
703 organization (D) and Programmed cell death (E) heatmaps in mouse system 48h after IAV
704 infection

705 **Figure S4: Flow cytometry gating strategy to describe resident memory lymphoid cells in**
706 **murine PCLS**

707 Examplary gating strategy is shown for a lymphoid cell panel

708 **Figure S5: Flow cytometry gating strategy to describe immune cells in human PCLS**

709 Examplary gating strategy is shown for A) Lymphoid cell panel B) Myeloid cell panel.

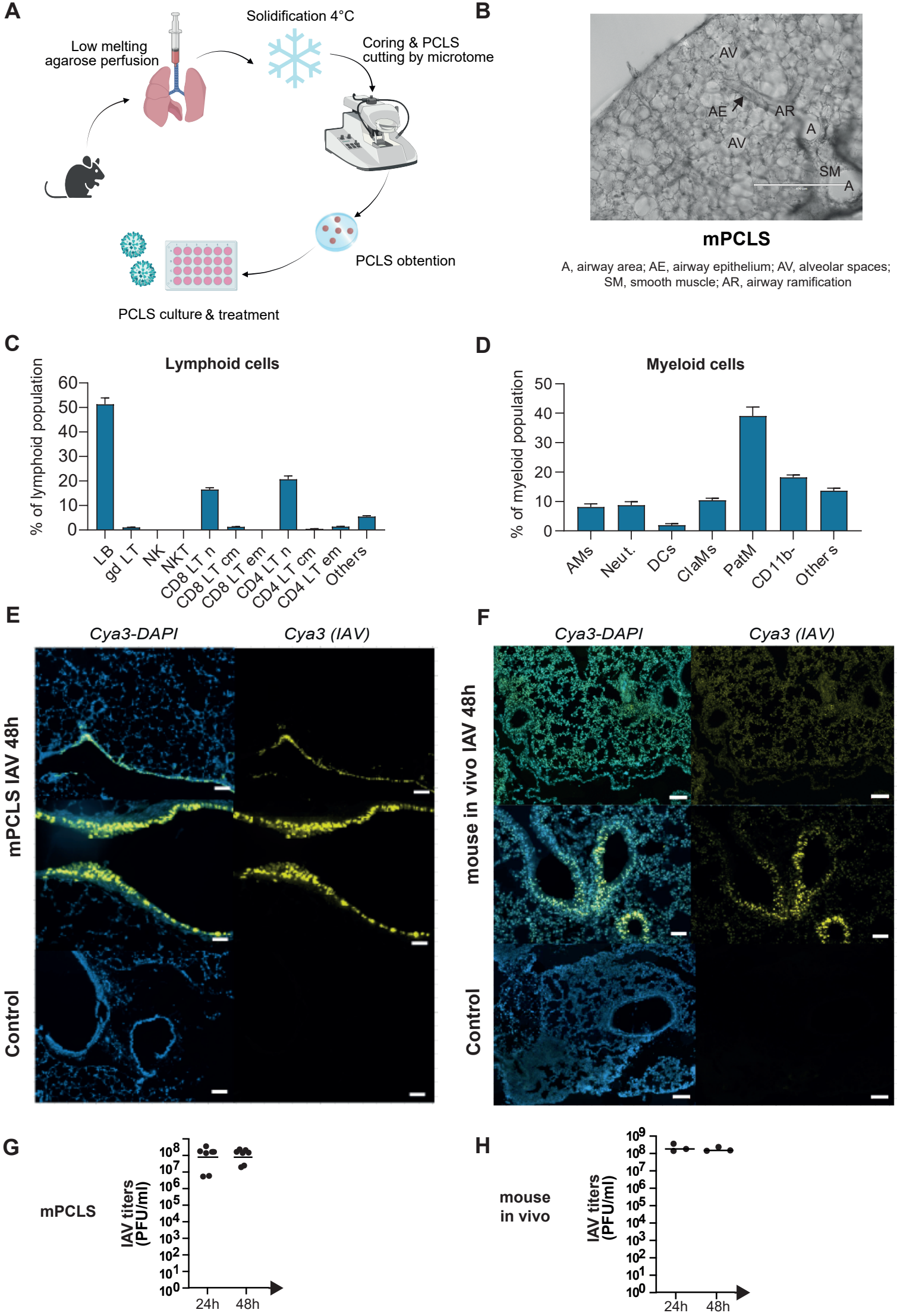
A
Solidification 4°C
Low melting agarose perfusion
Coring & PCLS cutting by microtome
PCLS obtention
PCLS culture & treatment
B
AV
AE
AR
A
AV
SM
A
mPCLS
A, airway area; AE, airway epithelium; AV, alveolar spaces; SM, smooth muscle; AR, airway ramification
C
Lymphoid cells
% of lymphoid population
60
50
40
30
20
10
0
LB
gd LT
NK
NKT
CD8 LT n
CD8 LT cm
CD8 LT em
CD4 LT n
CD4 LT cm
CD4 LT em
Others
D
Myeloid cells
% of myeloid population
50
40
30
20
10
0
AMs
Neut.
DCs
ClaMs
PatM
CD11b-
Others
E
Cya3-DAPI
Cya3 (IAV)
mPCLS IAV 48h
Control
F
Cya3-DAPI
Cya3 (IAV)
mouse in vivo IAV 48h
Control
G
mPCLS
IAV titers (PFU/ml)
10^8
10^7
10^6
10^5
10^4
10^3
10^2
10^1
10^0
24h
48h
H
mouse in vivo
IAV titers (PFU/ml)
10^9
10^8
10^7
10^6
10^5
10^4
10^3
10^2
10^1
10^0
24h
48h

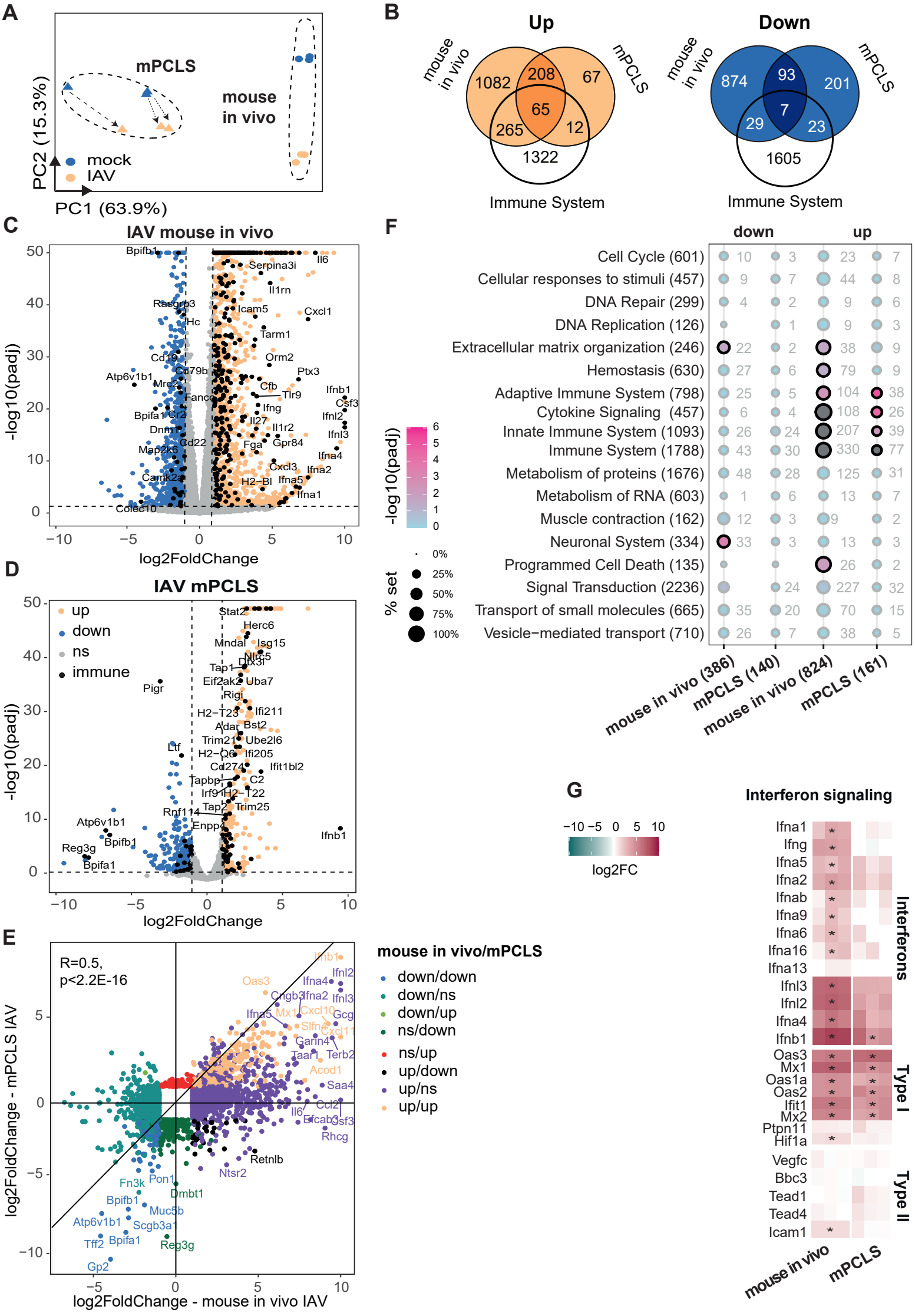
A
mPCLS
mouse in vivo
mock
IAV
PC2 (15.3%)
PC1 (63.9%)
B
Up
mouse in vivo
mPCLS
1082
208
67
65
265
12
1322
Immune System
Down
mouse in vivo
mPCLS
874
93
201
7
29
23
1605
Immune System
C
IAV mouse in vivo
-log10(padj)
log2FoldChange
D
IAV mPCLS
up
down
ns
immune
-log10(padj)
log2FoldChange
E
R=0.5,
p<2.2E-16
log2FoldChange - mPCLS IAV
log2FoldChange - mouse in vivo IAV
mouse in vivo/mPCLS
down/down
down/ns
down/up
ns/down
ns/up
up/down
up/ns
up/up
F
down
up
Cell Cycle (601)
Cellular responses to stimuli (457)
DNA Repair (299)
DNA Replication (126)
Extracellular matrix organization (246)
Hemostasis (630)
Adaptive Immune System (798)
Cytokine Signaling (457)
Innate Immune System (1093)
Immune System (1788)
Metabolism of proteins (1676)
Metabolism of RNA (603)
Muscle contraction (162)
Neuronal System (334)
Programmed Cell Death (135)
Signal Transduction (2236)
Transport of small molecules (665)
Vesicle−mediated transport (710)
mouse in vivo (386)
mPCLS (140)
mouse in vivo (824)
mPCLS (161)
-log10(padj)
% set
0%
25%
50%
75%
100%
G
log2FC
Interferon signaling
Interferons
Type I
Type II
mouse in vivo
mPCLS

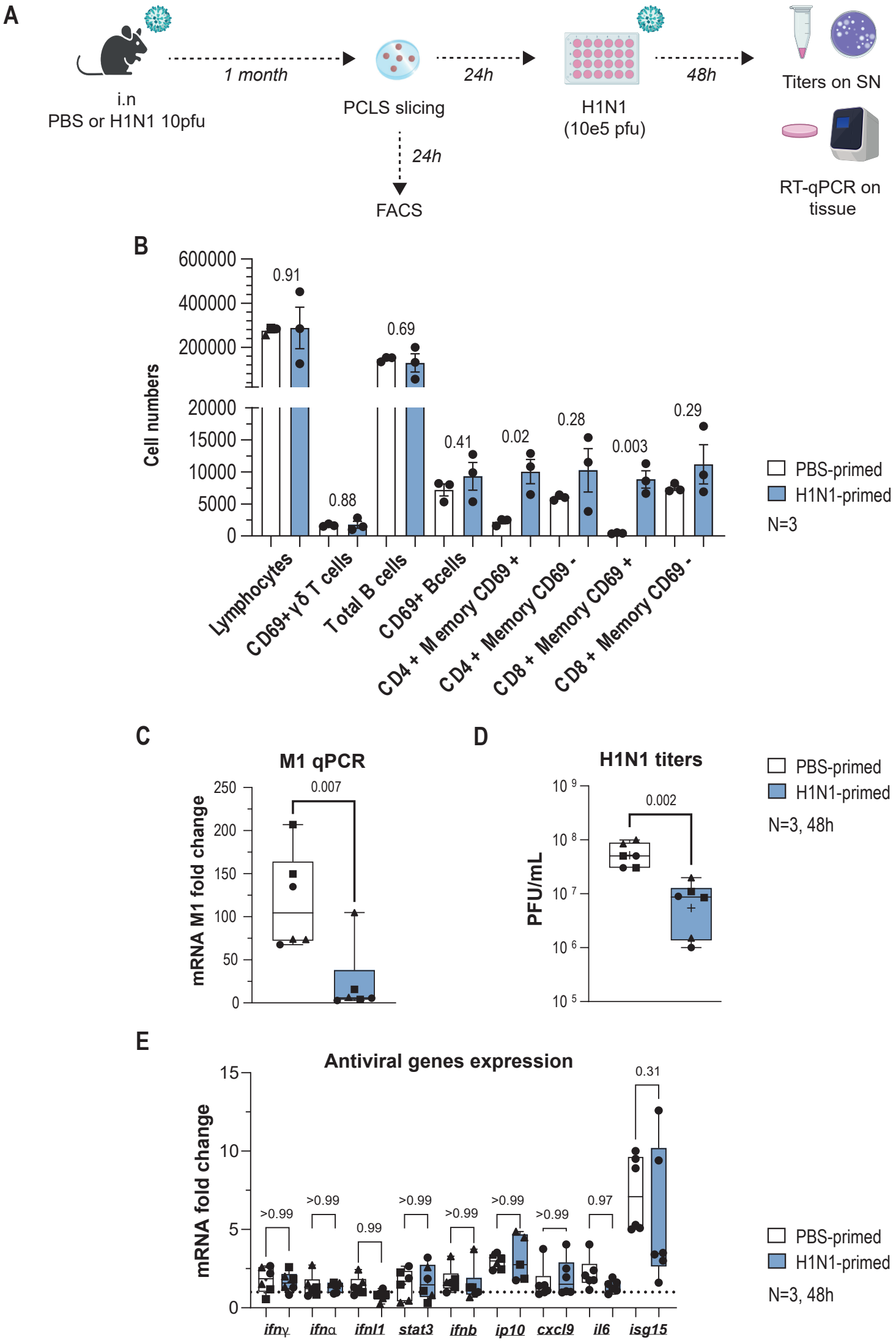
A
i.n
PBS or H1N1 10pfu
1 month
PCLS slicing
24h
H1N1
(10e5 pfu)
48h
Titers on SN
RT-qPCR on tissue
24h
FACS
B
Cell numbers
600000
400000
200000
20000
15000
10000
5000
0
0.91
0.69
0.88
0.41
0.02
0.28
0.003
0.29
Lymphocytes
CD69+γδ T cells
Total B cells
CD69+ Bcells
CD4+ Memory CD69+
CD4+ Memory CD69-
CD8+ Memory CD69+
CD8+ Memory CD69-
PBS-primed
H1N1-primed
N=3
C
M1 qPCR
mRNA M1 fold change
250
200
150
100
50
0
0.007
D
H1N1 titers
PFU/mL
10 9
10 8
10 7
10 6
10 5
0.002
PBS-primed
H1N1-primed
N=3, 48h
E
Antiviral genes expression
mRNA fold change
15
10
5
0
>0.99
>0.99
0.99
>0.99
>0.99
>0.99
>0.99
0.97
0.31
ifnγ
ifnα
ifnl1
stat3
ifnb
ip10
cxcl9
il6
isg15
PBS-primed
H1N1-primed
N=3, 48h

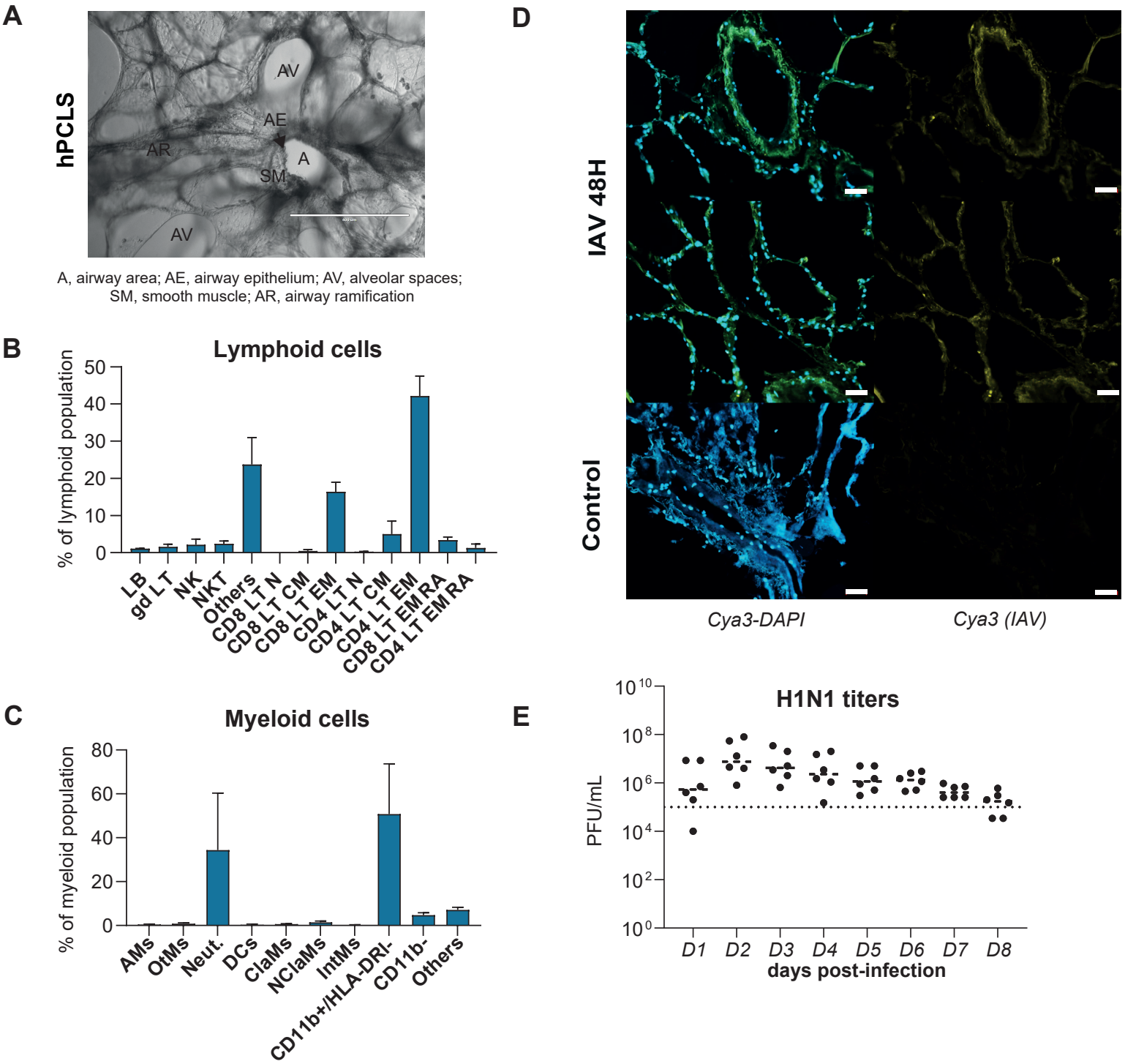
A
hPCLS
AV
AE
AR
A
SM
AV
A, airway area; AE, airway epithelium; AV, alveolar spaces;
SM, smooth muscle; AR, airway ramification
B
Lymphoid cells
% of lymphoid population
50
40
30
20
10
0
LB
gd LT
NK
NKT
Others
CD8 LT N
CD8 LT CM
CD8 LT EM
CD4 LT N
CD4 LT CM
CD4 LT EM
CD8 LT EMRA
CD4 LT EMRA
C
Myeloid cells
% of myeloid population
80
60
40
20
0
AMs
OtMs
Neut.
DCs
ClaMs
NClaMs
IntMs
CD11b+/HLA-DRl-
CD11b-
Others
D
IAV 48H
Control
Cya3-DAPI
Cya3 (IAV)
E
H1N1 titers
PFU/mL
10^{10}
10^{8}
10^{6}
10^{4}
10^{2}
10^{0}
D1
D2
D3
D4
D5
D6
D7
D8
days post-infection

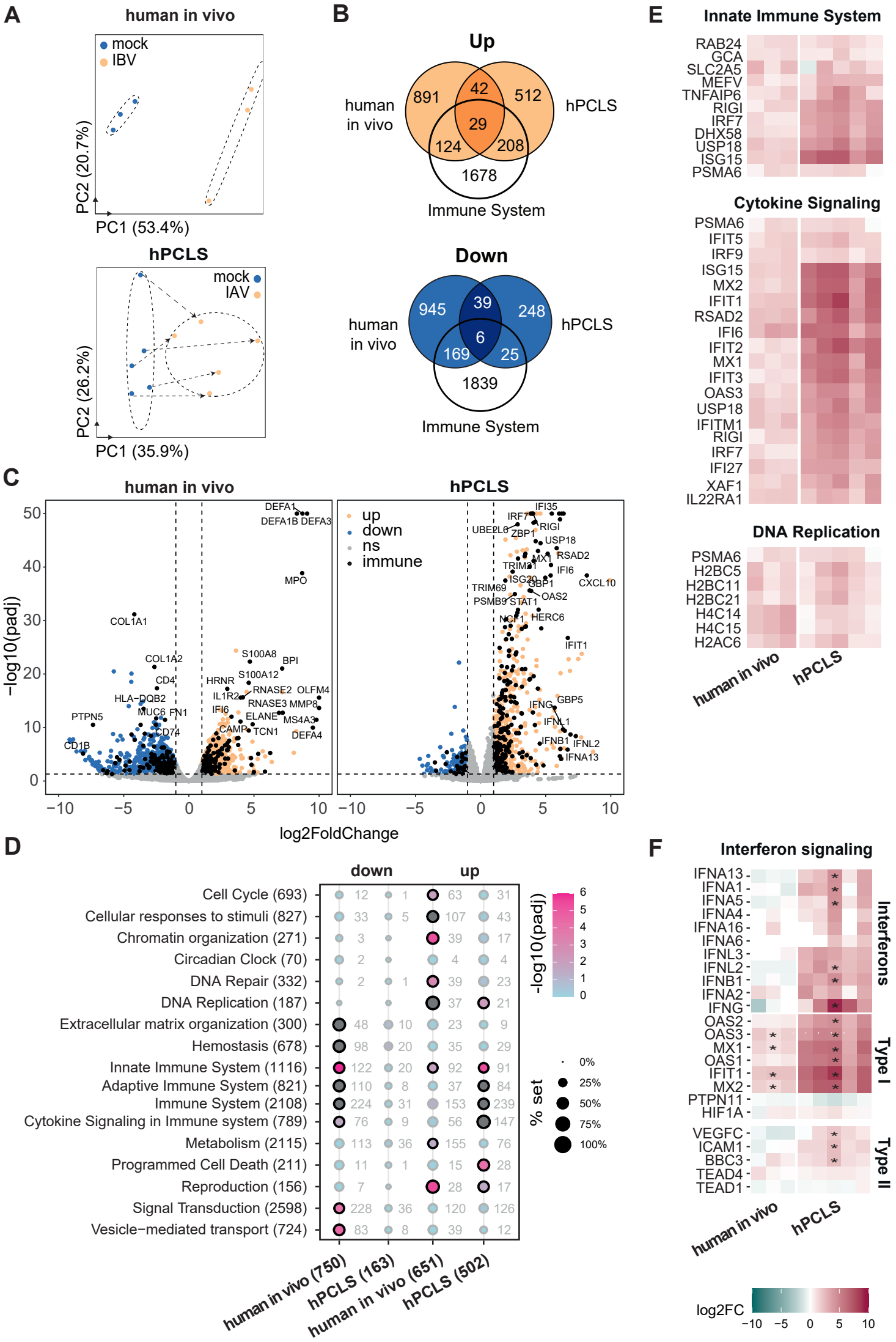
A
human in vivo
mock
IBV
PC2 (20.7%)
PC1 (53.4%)
hPCLS
mock
IAV
PC2 (26.2%)
PC1 (35.9%)
B
Up
human in vivo
hPCLS
891
42
512
29
124
208
1678
Immune System
Down
human in vivo
hPCLS
945
39
248
6
169
25
1839
Immune System
C
human in vivo
hPCLS
up
down
ns
immune
−log10(padj)
log2FoldChange
DEFA1
DEFA1B DEFA3
MPO
COL1A1
COL1A2
CD4
HLA−DQB2
MUC6 FN1
PTPN5
CD74
CD1B
S100A8
BPI
S100A12
HRNR
RNASE2 OLFM4
IL1R2
RNASE3 MMP8
IFI6
ELANE
MS4A3
CAMP
TCN1
DEFA4
IFI35
IRF7
RIGI
UBE2L6
ZBP1
USP18
MX1
RSAD2
TRIM21
IFI6
ISG20
GBP1
CXCL10
TRIM69
OAS2
PSMB9
STAT1
NCF1
HERC6
IFIT1
IFNG
GBP5
IFNL1
IFNB1
IFNL2
IFNA13
D
down
up
Cell Cycle (693) 12 1 63 31
Cellular responses to stimuli (827) 33 5 107 43
Chromatin organization (271) 3 39 17
Circadian Clock (70) 2 4 4
DNA Repair (332) 2 1 39 23
DNA Replication (187) 37 21
Extracellular matrix organization (300) 48 10 23 9
Hemostasis (678) 98 20 35 29
Innate Immune System (1116) 122 20 92 91
Adaptive Immune System (821) 110 8 37 84
Immune System (2108) 224 31 153 239
Cytokine Signaling in Immune system (789) 76 9 56 147
Metabolism (2115) 113 36 155 76
Programmed Cell Death (211) 11 1 15 28
Reproduction (156) 7 28 17
Signal Transduction (2598) 228 36 120 126
Vesicle−mediated transport (724) 83 8 39 12
human in vivo (750)
hPCLS (163)
human in vivo (651)
hPCLS (502)
−log10(padj)
% set
0%
25%
50%
75%
100%
E
Innate Immune System
RAB24
GCA
SLC2A5
MEFV
TNFAIP6
RIGI
IRF7
DHX58
USP18
ISG15
PSMA6
Cytokine Signaling
PSMA6
IFIT5
IRF9
ISG15
MX2
IFIT1
RSAD2
IFI6
IFIT2
MX1
IFIT3
OAS3
USP18
IFITM1
RIGI
IRF7
IFI27
XAF1
IL22RA1
DNA Replication
PSMA6
H2BC5
H2BC11
H2BC21
H4C14
H4C15
H2AC6
human in vivo
hPCLS
F
Interferon signaling
IFNA13
IFNA1
IFNA5
IFNA4
IFNA16
IFNA6
IFNL3
IFNL2
IFNB1
IFNA2
IFNG
Interferons
OAS2
OAS3
MX1
OAS1
IFIT1
MX2
Type I
PTPN11
HIF1A
VEGFC
ICAM1
BBC3
TEAD4
TEAD1
Type II
human in vivo
hPCLS
log2FC
−10 −5 0 5 10

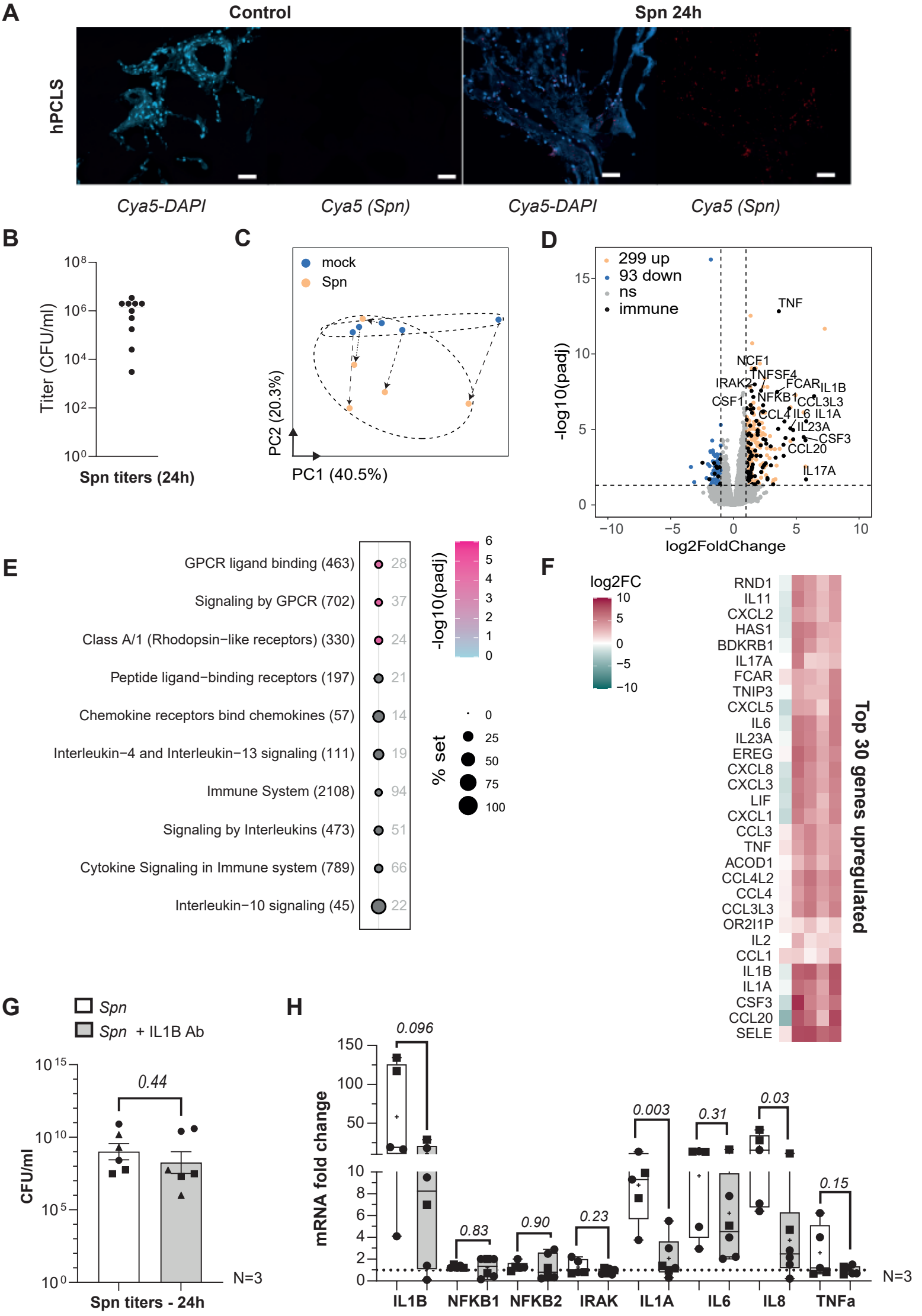
A
Control
Spn 24h
hPCLS
Cya5-DAPI
Cya5 (Spn)
Cya5-DAPI
Cya5 (Spn)
B
Titer (CFU/ml)
Spn titers (24h)
C
mock
Spn
PC2 (20.3%)
PC1 (40.5%)
D
299 up
93 down
ns
immune
-log10(padj)
log2FoldChange
TNF
NCF1
TNFSF4
IRAK2
FCAR
IL1B
CSF1
NFKB1
CCL3L3
CCL4
IL6
IL1A
IL23A
CSF3
CCL20
IL17A
E
GPCR ligand binding (463)
Signaling by GPCR (702)
Class A/1 (Rhodopsin−like receptors) (330)
Peptide ligand−binding receptors (197)
Chemokine receptors bind chemokines (57)
Interleukin−4 and Interleukin−13 signaling (111)
Immune System (2108)
Signaling by Interleukins (473)
Cytokine Signaling in Immune system (789)
Interleukin−10 signaling (45)
-log10(padj)
% set
F
log2FC
Top 30 genes upregulated
RND1
IL11
CXCL2
HAS1
BDKRB1
IL17A
FCAR
TNIP3
CXCL5
IL6
IL23A
EREG
CXCL8
CXCL3
LIF
CXCL1
CCL3
TNF
ACOD1
CCL4L2
CCL4
CCL3L3
OR2I1P
IL2
CCL1
IL1B
IL1A
CSF3
CCL20
SELE
G
Spn
Spn + IL1B Ab
CFU/ml
0.44
N=3
Spn titers - 24h
H
mRNA fold change
0.096
0.83
0.90
0.23
0.003
0.31
0.03
0.15
N=3
IL1B
NFKB1
NFKB2
IRAK
IL1A
IL6
IL8
TNFa